Activating *RAC1* variants in the switch II region cause a developmental syndrome and alter neuronal morphology

Siddharth Banka,[1,2] Abigail Bennington,[3] Martin J. Baker,[4,5] Ellen Rijckmans,[6,7] Giuliana D. Clemente,[3,8] Nurhuda Mohamad Ansor,[3,9] Hilary Sito,[3] Pritha Prasad,[3] Kwame Anyane-Yeboa,[10] Lauren Badalato,[11] Boyan Dimitrov,[12] David Fitzpatrick,[13] Anna C. E. Hurst,[14] Anna C. Jansen,[7,15] Melissa A. Kelly,[16] Ian Krantz,[17] Claudine Rieubland,[18] Meredith Ross,[10] Natasha L. Rudy,[14] Javier Sanz,[18] Katrien Stouffs,[7,12] Zhuo Luan Xu,[17] Angeliki Malliri,[5] Marcelo G. Kazanietz[4] and Tom H. Millard[3]

1 Division of Evolution, Infection and Genomics, School of Biological Sciences, Faculty of Biology, Medicine and Health, University of Manchester, Manchester M13 9PL, UK

2 Manchester Centre For Genomic Medicine, University of Manchester, St Mary's Hospital, Manchester Academic Health Science Centre, Manchester M13 9WL, UK

3 Division of Developmental Biology & Medicine, Faculty of Biology, Medicine and Health, University of Manchester M13 9PL, UK

4 Department of Systems Pharmacology and Translational Therapeutics, Perelman School of Medicine, University of Pennsylvania, Philadelphia, PA, USA

5 Cell Signalling Group, Cancer Research UK Manchester Institute, The University of Manchester, Alderley Park, Macclesfield SK10 4TG, UK

6 Department of Pediatrics, UZ Brussel, Brussels, Belgium

7 Neurogenetics Research Group, Vrije Universiteit Brussel, Brussels, Belgium

8 School of Biochemistry, University of Bristol, Bristol BS8 1TD, UK

9 Advanced Medical and Dental Institute, Universiti Sains Malaysia, 13200 Kepala Batas, Penang, Malaysia

10 Columbia University Medical Center, New York 10032, USA

11 Department of Pediatrics, School of Medicine, Kingston General Hospital, Queen's University, Kingston, ON, Canada

12 Centre for Medical Genetics, UZ Brussel, Brussels, Belgium

13 MRC Human Genetics Unit, IGMM, University of Edinburgh, Edinburgh, UK

14 University of Alabama at Birmingham, Birmingham, Alabama, USA

15 Pediatric Neurology Unit, Department of Pediatrics, UZ Brussel, Brussels, Belgium

16 HudsonAlpha Clinical Services Lab, Huntsville, Alabama, USA

17 Roberts Individualized Medical Genetics Center, Children's Hospital of Philadelphia, Philadelphia, PA, USA

18 Department of Human Genetics, Inselspital, Bern University Hospital, University of Bern, Switzerland

Correspondence to: Tom H. Millard

University of Manchester, Faculty of Biology, Medicine and Health, Michael Smith Building, Oxford Road, Manchester M13 9PT, UK

E-mail: Tom.Millard@manchester.ac.uk

Correspondence may also be addressed to: Siddharth Banka

Manchester Centre For Genomic Medicine, University of Manchester, St Mary's Hospital, Manchester Academic Health Science Centre, Oxford Road, Manchester M13 9WL, UK

E-mail: Siddharth.Banka@manchester.ac.uk

Running title: Activating *RAC1* variants

Abstract

RAC1 is a highly conserved Rho GTPase critical for several cellular and developmental processes. D*e novo* missense *RAC1* variants cause a highly variable neurodevelopmental disorder. Some of these variants have been previously shown to have a dominant negative effect. Most previously reported patients with this disorder have either severe microcephaly or severe macrocephaly.

Here we describe eight patients with pathogenic missense *RAC1* variants affecting residues between Q61 and R68 within the switch II region of RAC1. These patients display variable combinations of developmental delay, intellectual disability, brain anomalies such as polymicrogyria, and cardiovascular defects with normocephaly or relatively milder micro- or macrocephaly. Pulldown assays, NIH3T3 fibroblasts spreading assays and staining for activated PAK1/2/3 and WAVE2 suggest that these variants increase RAC1 activity and over-activate downstream signalling targets. Axons of neurons isolated from *Drosophila* embryos expressing the most common of the activating variants are significantly shorter, with an increased density of filopodial protrusions. *In vivo*, these embryos exhibit frequent defects in axonal organization. Class IV dendritic arborisation neurons expressing this variant exhibit a significant reduction in the total area of the dendritic arbour, increased branching and failure of self-avoidance. RNAi knock down of the WAVE regulatory complex component Cyfip significantly rescues these morphological defects.

These results establish that activating substitutions affecting residues Q61-R68 within the switch II region of RAC1 cause developmental syndrome. Our findings reveal that these variants cause altered downstream signalling resulting in abnormal neuronal morphology and reveal the WAVE regulatory complex/Arp2/3 pathway as a possible therapeutic target for activating RAC1 variants. These insights

also have the potential to inform the mechanism and therapy for other disorders caused by variants in genes encoding other Rho GTPases, their regulators and downstream effectors.

Keywords: RAC1; small GTPases; intellectual disability; polymicrogyria; WAVE regulatory complex

Abbreviations: CA = constitutively active; cIVda = class IV dendritic arborisation; DN = dominant negative; FasII **=** Fasciculin II; GAP = GTPase activating protein; NDD = Neurodevelopmental disorder; PAK = p21-activated kinase; WRC **=** WAVE Regulatory Complex; WT = Wild-type

Introduction

RAC1 is a highly conserved Rho GTPase that switches between an inactive GDP-bound state and an active GTP-bound state in which it can bind to and regulate the function of numerous cellular proteins.[1] RAC1 plays several roles in the development and function of the nervous system including regulation of neuronal morphology and migration.[2] Functional importance of *RAC1* is emphasised by its high mutational constraint in the general population.[3] We recently described *de novo* missense *RAC1* variants, spread across the gene, resulting in a highly variable neurodevelopmental disorder (RAC1-NDD) (OMIM 617751).[4] Notably, the head circumferences of the patients with RAC1-NDD ranged from -5SD to +4.5SD. We provisionally divided RAC1-NDD patients into three broad phenotype-based groups of microcephalic, normocephalic and macrocephalic. We showed that some 'microcephaly *RAC1* variants' are likely to have dominant-negative effects. Macrocephaly was noted in two patients, both with RAC1 substitutions affecting the residue V51. Normocephaly was noted in only one patient with a *RAC1* Y64D variant. This variant was located in switch II, a region of RAC1 that undergoes significant structural changes when RAC1 transitions between GTP and GDP bound states. This Y64D substitution was the only variant we found to be likely activating in our previous study.

Here, we describe eight patients with five distinct *RAC1* variants leading to substitution of three different residues all within a region of switch II and show that this group of variants result in a developmental syndrome. Using Rac1-GTP pulldown assays, immunofluorescence and NIH3T3 spreading assays we demonstrate that substitutions at these sites result in a higher proportion of RAC1 in the active GTP-bound state, increased RAC1 activity and signalling via multiple downstream effectors, including the RAC1/WAVE Regulatory Complex (WRC) /Arp2/3 pathway, and altered cell morphology. Using a *Drosophila* model we show that the most common of these variants, Y64D, induces morphological changes in embryonic neurons, causes axon fasciculation defects in the embryonic

central nervous system (CNS), and increases branching of sensory neurons. Finally, we show that Rac1-Y64D-induced neuronal branching defects can be rescued in *Drosophila* by knockdown of the WRC component Cyfip, homolog of human CYFIP1/2.

Materials and methods

Patient identification

We identified patients with *RAC1* missense variants affecting the residues in the switch II region of RAC1 through the Deciphering Developmental Disorders study[5] and via personal collaborations. The Central Manchester and the Cambridge South NHS Research Ethics Committees approved this study (02/CM/238 and 10/H0305/83 respectively). InterVar (http://wintervar.wglab.org/) was used to apply the 2015 American College of Medical Genetics and Genomics (ACMG) guidelines for variant interpretation.[6] A customized proforma was completed to collate relevant clinical information. Informed consent from patients or their legal representatives was obtained in all cases.

Rac1-GTP pulldown assays

Mutations were introduced into the coding region of human *RAC1* using Quikchange Lightning (Aligent) according to the manufacturer's instructions and subcloned in pRK5-myc using *Bam* HI and *Eco* RI. RAC1-GTP pulldown assays were performed as previously described.[7] Briefly, HEK293 cells were transfected using Jet-OPTIMUS transfection reagent (Polyplus). Transfected cells were then incubated for 24 hour before being lysed and active RAC1 isolated using the recombinant CRIB domain of PAK fused to GST. The ratio of isolated myc-RAC1-GTP to total myc-RAC1 was then assessed using Western blotting, probing for the myc-tag (Cell Signaling Technologies #2278) followed by a goat anti-rabbit HRP secondary (BioRad) and visualized using enhanced chemiluminescence.

NIH3T3 spreading assays and immunofluorescence

Subconfluent NIH3T3 cells in a 24 well plate were transfected with RAC1 variants in pRK5-myc using Fugene 6 transfection reagent (Promega) according to the manufacturer's instructions. 24 hr later cells were trypsinised and replated on 13mm coverslips coated with fibronectin. 30 min after replating, cells were fixed with 4% formaldehyde in PBS, then permeabilised with 0.1% Triton X-100 in PBS. Cells were then blocked with 1% BSA in PBS followed by incubation with primary antibodies in blocking buffer and secondary antibodies in PBS. Finally, coverslips were mounted using Prolong Gold antifade reagent with DAPI (Invitrogen) and imaged using a Leica DL600 widefield compound microscope with a 63x/1.40NA oil objective. Antibodies used: Anti-myc mouse monoclonal (9E10) (Sigma-Aldrich) 1:500; Anti-phospho-Ser141 PAK-1/2/3 rabbit polyclonal (ThermoFisher, 44-940G) 1:100; Anti-WAVE-2 (D2C8) rabbit monoclonal antibody (Cell Signalling Technology, 3659) 1:100; Alexa-568 donkey anti-rabbit secondary antibody (Invitrogen) 1:500; Alexa-488 donkey anti-mouse (Invitrogen) 1:500; Alexa-568-phalloidin (Invitrogen) 1:500.

Image analysis

All image analysis was performed using ImageJ. Transfected cells were identified by viewing myc-RAC1 staining and cells with moderate expression levels selected for analysis. The ImageJ "threshold" function to segment cell perimeters in the phalloidin channel, then the "analyse particles" function was used to calculate circularity index ($4\pi \times \text{area}/\text{perimeter}^2$). To quantify active-PAK fluorescence a 17 μm^2 region of interest was selected close to the cell periphery using the myc-RAC1 channel without viewing the active-PAK channel to avoid bias. The total fluorescence (raw integrated density) in this region of interest in the active-PAK channel was then measured. Background fluorescence measured in an area of the coverslip with no cells was subtracted from the resulting value. Three independent repeats were

performed for all cell culture experiments. Statistical analysis was carried using Graphpad Prism, and images were processed and compiled using ImageJ, Adobe Photoshop and Adobe Illustrator.

Drosophila stocks

The following fly lines were obtained from Bloomington *Drosophila* stock center: elav-Gal4 (stock 8760), ppk-Gal4 (stock 32079), UAS-CD8-mCherry (stock 27392), UAS-Rac1 (stock 6293) and UAS-*Cyfip*-RNAi (stock 38294). To generate flies expressing Rac1-Y64D under UAS-Gal4 control, the coding region of *Drosophila Rac1* was amplified from a cDNA clone and cloned into pGEMT (Promega). Mutagenesis to introduce Y64D was carried out using Quikchange Lightning (Aligent), and the resulting construct subcloned into pUASp using *Not* I and *Xba* I. Transgenic flies were generated using the resulting plasmid by BestGene Inc. (California, USA).

Drosophila primary neuron culture and immunocytochemistry

Drosophila primary neurons were cultured as described previously.[8] In brief, 24 stage 11 embryos were dechorioned with 50% bleach, washed briefly with 70% ethanol, then culture medium (Schneider's medium (Gibco), 20% fetal calf serum (Gibco)) and homogenized using a micro-pestle in Hanks' balanced salt solution (Gibco) supplemented with collagenase, dispase and penicillin/streptomycin (Gibco) for 5 min at 37 °C. Cells were washed with culture medium, pelleted and resuspended in fresh culture medium. The cell suspension was plated on glass coverslips and incubated at 26 °C for six hours, then fixed with 4% formaldehyde in PBS. Following permeabilization with 0.1 % Triton X-100 in PBS (PBT), cell cultures were stained with mouse anti-tubulin (Sigma Aldrich, T9026) at 1:1000 in PBT, followed by anti-mouse Alexa-488 (Invitrogen) at 1:500 and Alexa-568-phalloidin (Invitrogen) at 1:200 in PBT then mounted in Prolong Gold containing DAPI (Thermofisher). Cultures were imaged using a Nikon A1R confocal microscope, 60x Plan-Apo VC oil objective. Images were analysed using ImageJ.

Drosophila embryo immunohistochemistry

Embryos were dechorionated by immersion in 50% sodium hypochlorite (Sigma Aldrich) for 2 min, washed with water, then fixed in 1:1 4% formaldehyde in PBS:heptane for 20 min at RT. The aqueous phase was removed and 1vol methanol added to the heptane phase. The tube was shaken for 1 min and the heptane/methanol removed. Embryos were washed with methanol then PBT, then blocked with 2% BSA in PBT. Embryos were stained with anti-FasII (DSHB) at 1:100 followed by anti-mouse Alexa-488 (Invitrogen) at 1:500, both in blocking solution then mounted in Prolong Gold containing DAPI (Thermofisher). Embryos were imaged using a Nikon A1R confocal microscope, 20x Plan-Apo VC objective. Images were analysed and processed using ImageJ and Adobe Photoshop. Segment scored positive for fasciculation defect if defect extends ≥ half segment length.

Imaging *Drosophila* larval sensory neurons

L3 *Drosophila* larvae were anesthesized using diethyl ether vapour, essentially as previously described.[9] Briefly, selected larvae were washed with water, dried, then placed with the lid of a 1.5ml Eppendorf tube, which was placed in a closed bottle containing cotton wool soaked in diethyl ether for 5 minutes. Anaesthetised larvae were then mounted between a slide and coverslip, with additional coverslips placed either side of the larvae to prevent their crushing. Images of cIVda neurons on the dorsal surface of the segments A1-A4 were collected using a Nikon A1R confocal microscope, 20x Plan-Apo VC dry objective. Images were analysed and processed using ImageJ and Adobe Photoshop.

Data availability

Experimental data will be shared on reasonable request from qualified investigators.

Results

Substitutions in the Q61-R68 region of RAC1 cause a developmental syndrome

Switch II comprises approximately residues 57-75 of RAC1 and is a conserved structural feature of small GTPases that undergoes a conformational change on exchange of GDP for GTP.[10] Based on our previous analysis of a single normocephalic patient with a Y64D *RAC1* variant, we hypothesised that some variants in the switch II region may cause a disorder distinct from the microcephalic and macrocephalic forms of RAC1-NDD.[4] Through collaborations and the DDD study, we identified eight patients (including the original patient in our previous study[4]) with missense variants affecting residues between Q61 and R68 of *RAC1* (Table 1). These included four patients with the identical Y64D variant and one patient each with Q61E, Y64C, R68S and R68G variants. In all individuals, where investigation of inheritance was possible, the variants were found to have occurred *de novo*. All the variants affect amino acids that are highly conserved across orthologs, paralogs and the wider RAS superfamily (Fig 1A). No variants affecting these residues are found in control databases. All variants affecting residues 61 or 64 were classified as pathogenic according to the ACMG variant interpretation guidelines (Supplementary Table S1). The two variants affecting the residue R68 were initially classified as variants of uncertain significance because both parents could not be tested to confirm the variants to be *de novo* in these cases (Table 1). However, if the results of functional studies described later in the manuscript are taken into account, these variants could be reclassified as likely pathogenic (Supplementary Table S1). Switch II is the primary binding site for upstream regulators and also contains the G3 box which is involved in GTP hydrolysis.[10] Q61, mutated to glutamate in one patient, has a well-established role in GTP hydrolysis and substitution of this residue has frequently been observed to activate small GTPases, including RAC1.[11-13] Y64 is not directly involved in nucleotide binding or hydrolysis, but its side chain is exposed on the

surface of switch II (Fig.1B), so substitution of this residue to aspartate or cysteine may affect the ability of RAC1 to interact with upstream regulators. The side chain of R68 is predicted to form hydrogen bonds with several other residues within and close to switch II (Fig. 1B), so substitution of R68 to glycine or serine is likely to alter the structure of switch II, potentially affecting GTP hydrolysis or interaction with upstream regulators. These data suggest that *RAC1* variants affecting the residues Q61, Y64 and R68 identified in this study are pathogenic or likely pathogenic.

Next, we studied the clinical phenotypes of the eight patients, including the one patient with Y64D we published previously. This cohort comprises of five females and three males with ages between 20 months to 15 years. Birth head circumference was known in only one case and was within the normal range. Most recent head circumferences were reported to be within normal range in six out of eight patients. One girl with R68S, born pre-maturely in 26th week of gestation, had mild microcephaly of -2.2 SD at 4y 5m of age. One boy with a Y64D variant had mild macrocephaly of +3.06 at 14y of age. Age of independent walking was delayed in five out of seven children for whom information on motor milestones was available. Although formal assessments were not available for these patients, the recruiting clinicians reported the cognitive delay or intellectual disabilities ranging from mild to severe in all patients. None of the affected individuals were reported to have epilepsy. Brain magnetic resonance scans (MRI), showed polymicrogyria in two patients, one with Y64C and one with the Y64D variant (Fig. 1C). Brain MRI scans were not performed in two individuals. Cardiovascular anomalies, such as ventricular septal defects, atrial septal defects and patent ductus arteriosus, were noted in 4/8 patients. The patient with Q61E variant was also noted to have significant obesity with weight of >6SD at the age of 2½ years.

Comparison with previously published V51 RAC1-NDD patients showed that, none of the patients in the current cohort had severe macrocephaly (Table 2). Comparison with previously published all other

(likely dominant negative) RAC1-NDD patients showed that none of the patients in the current cohort had severe microcephaly or epilepsy (Table 2). Although the patient numbers in the three groups are still small, collectively, these data suggest that *RAC1* variants affecting the residues Q61, Y64 and R68 in the switch II region result in a developmental syndrome with a phenotypic spectrum that is different from RAC1-NDD caused by other known *RAC1* variants.

RAC1 variants affecting Q61-R68 of switch II increase RAC1 activity

To investigate whether the variants described above alter the proportion of cellular RAC1 in an active state, we performed RAC1-GTP pulldown assays using lysates of unstimulated HEK293 cells expressing patient variants or control *RAC1* constructs. Three of the five patient variants were selected for this analysis: Y64D, Y64C and R68G. The level of RAC1-GTP pulled down by the RAC binding domain of PAK was analysed by western blot and normalised to the total level of RAC1 in the lysate. A previously characterised constitutively active variant of RAC1 (Q61L) exhibited increased levels of GTP-binding relative to RAC1 wild-type (WT), while a known dominant negative variant (T17N) exhibited reduced GTP binding. All three of the patient variants analysed exhibited significantly increased GTP binding relative to RAC1-WT (Figure 2A-B). The increase in RAC1-GTP levels varied between the different variants, with the R68G variant exhibiting the largest increase. One of the two patient variants not analysed here; Q61E, has previously been shown to increase RAC1-GTP levels in a similar pulldown assay[13]. We, therefore, conclude that patient variants affecting residues Q61, Y64 and R68 all increase levels of the activated GTP-bound form of RAC1.

RAC1 promotes the formation of lamellipodia and membrane ruffles around the cell periphery as cells spread, so the morphology of spreading cells is a useful cellular readout of RAC1 function. Constitutively active RAC1 (Q61L) promotes the formation of lamellipodia around the whole cell periphery, causing fibroblasts to exhibit a circular morphology, while dominant negative RAC1 (T17N) suppresses

lamellipodia, leading to a stellate morphology dominated by filopodia (Fig. 2C,E). We expressed RAC1-Y64D, -Y64C and -R68G in NIH3T3 fibroblasts and examined their effect on the morphology of cells spreading on a fibronectin-coated surface. We found that cells expressing these variants typically exhibited a circular morphology reminiscent of cells expressing constitutively active RAC1, with the cell periphery dominated by lamellipodia and membrane ruffles (Fig. 2C,E). Cell circularity index ($4\pi\times$area/perimeter^2) provides a simple means of quantifying cell morphology, and we found that RAC1-Y64D, -Y64C and -R68G all induced significant increased circularity relative to RAC1-WT, with circularity values for Y64C and R68G close to those induced by Q61L (Fig. 2D). The variants all exhibited increased localisation to the cell periphery relative to RAC1-WT (Fig. 2C, arrows), and this peripheral localisation was particularly pronounced for the Y64D and R68G variants.

Collectively, these data suggest that all the patient variants studied here increase the proportion of cellular RAC1 in an active GTP-bound state, increase RAC1 activity in cellular conditions and alter cell morphology.

Activating RAC1 switch II variants promote activation of downstream WRC and PAK signalling in fibroblasts

The WAVE regulatory complex is a downstream effector of RAC1 involved in regulating cell morphology in a variety of cell types including fibroblasts and neurons.[14,15] Binding of active RAC1 enables the WRC to activate the Arp2/3 complex, a nucleator of actin filaments,[16,17] and this RAC1/WRC/Arp2/3 pathway is implicated in regulating lamellipodia assembly in fibroblasts and axonal growth as well as initiation of collateral branches on axons and dendrites in neurons.[14,15,18] To test the effect of expressing the activating switch II variants on this signalling pathway, we stained spreading NIH3T3 fibroblasts with antibodies against WAVE2, a component of the WRC. In cells expressing WT or dominant negative RAC1,

WAVE2 was detected in the perinuclear region of the cell, but rarely at or close to the cell periphery. By contrast, cells expressing constitutively active RAC1, RAC1-Y64D, Y64C and R68G exhibited prominent WAVE2 localisation at the cell periphery (Fig. 3A, arrowheads), consistent with increased recruitment and activation of the WRC at the lamellipodial leading edge by the activating switch II variants.

The p21-activated kinase (PAK) family of protein kinases are activated by binding of active RAC1 and are implicated in regulating a variety of cellular processes including cell survival, proliferation and metabolism.[19] To test if this pathway is stimulated by the activating switch II variants we stained NIH3T3 fibroblasts expressing Y64D, Y64C and R68G with an antibody specific for the activated form of PAK1/2/3 phosphorylated at S141. While some staining was detected for activated PAK in cells expressing WT or dominant negative RAC1, this staining was restricted to the perinuclear region (Figure 3B). By contrast, activated PAK was detected throughout cells expressing constitutive active RAC1 and all the switch II variants tested, including punctate accumulations at and close to the cell periphery (Fig. 3B, arrowheads), where little or no active PAK was observed in cells expressing wild-type or dominant negative RAC1 (Fig 3B). Quantification of activated PAK staining close to the cell periphery suggested that levels of activated PAK were significantly elevated in this region for all switch II variants tested relative to wild-type RAC1, with levels highest for Y64C and R68G (Fig. 3C).

Collectively, these data provide further evidence that all the activating switch II variants studied here increase signalling through multiple downstream pathways including the WRC and PAK family kinases.

Rac1-Y64D induces morphological changes in *Drosophila* embryonic neurons

Given that all the activating switch II variants tested induce significant morphological changes in fibroblasts (Fig. 2C-E), we hypothesised that these variants may also alter the morphology of neurons and that this could contribute to disease phenotypes. Model organism studies have previously

demonstrated a variety of defects in neuronal morphology, including axonal misrouting and altered dendritic branching when RAC1 function is impaired.[2,20,21] The *Drosophila* homolog of RAC1, named Rac1, is 92% identical to its human equivalent and *Drosophila* has proved an excellent model for dissecting the functions of RAC1 in the nervous system,[15,20,22] so we chose this system to model the effects of activating switch II variants on neuronal morphology. Since Y64D is the most frequently observed variant in our cohort, it was chosen as an exemplar for activating switch II variants in this analysis. We thus generated a *Drosophila* strain harbouring a transgenic copy of *Drosophila* Rac1-Y64D under the control of the conditional UAS-Gal4 system, allowing targeted expression of this variant.

To examine the effect of Rac1-Y64D on axonal growth and morphology, we isolated neurons from stage 11 embryos expressing Rac1-Y64D under the control of the pan-neuronal elav-Gal4 driver and allowed the neurons to grow in culture for 6 hours. At this developmental stage, axons are just beginning to extend,[8] allowing us to capture the earliest effects of Rac1-Y64D on axonal growth and morphology. We found that the axons of neurons expressing Rac1-Y64D were around 2-fold significantly shorter than controls or those expressing Rac1-WT (Fig. 4A,B). Interestingly, Rac1-Y64D expression also resulted in an increase in the density of filopodial protrusions along the axon shaft, structures previously identified as precursors of collateral axonal branches (Fig. 4A,C, arrows).[18] These results suggest that Rac1-Y64D reduces the rate of axonal extension and promotes increased formation of collateral branch precursors.

Rac1-Y64D induces axon fasciculation defects in the *Drosophila* embryonic CNS

Our finding that axonal growth and morphology is perturbed in cultured neurons expressing Rac1-Y64D prompted us to investigate whether we could detect axonal defects in the intact embryonic nervous system. To examine axonal organization within the central nervous system, we stained embryos expressing this Rac1 variant under the control of the pan-neuronal driver elav-Gal4 with an antibody against Fasciculin II (FasII). The axons of neurons expressing FasII bundle into six fascicles that run

longitudinally within the nerve cord and any deviation from this arrangement is indicative of defects in axonal morphology or routing.[22] We found that while expression of UAS-Rac1-WT did not cause any obvious changes in the fasciculation of FasII positive axons, Rac1-Y64D expression resulted in frequent defects in axonal organization, including absence of fascicles, crossing of axons between fascicule tracks and defasciculation of axons (Fig. 4D,E).

Rac1-Y64D increases branching of sensory neurons

Since our data suggested that Rac1-Y64D may increase the formation of neuronal branch precursors, we investigated the effect of this variant on branching in more detail using an established model system for this process; class IV dendritic arborisation (cIVda) neurons.[15] This neuron class forms highly branched dendritic arbors, but since they exhibit self-avoidance and tiling, the morphology of individual cells can be accurately imaged and analysed in vivo.[23] Rac1-Y64D was expressed specifically in cIVda neurons using the ppk-Gal4 driver alongside a fluorescent membrane marker to allow the dendritic arbor of these cells to be easily visualized. Expression of Rac1-Y64D resulted in significant changes in the morphology of cIVda neurons (Fig. 5A,B). Firstly, the total area of the dendritic arbour was reduced in Rac1-Y64D expressing cells. Secondly, the density of branching close to the cell body was elevated compared to controls (Fig. 5D,E). Thirdly, crossing over of dendrites was observed, demonstrating failure of self-avoidance, suggesting defective dendrite pathfinding.

Rac1-Y64D-induced neuronal branching defects can be rescued by knockdown of the WRC component Cyfip

A recent report demonstrated that dendritic branching by cIVda neurons is initiated by activation of the actin-nucleating Arp2/3 complex downstream of Rac1 and the WRC.[15] Since our cell culture studies had suggested that Rac1-Y64D increases WRC activation, we hypothesized that the increased branching

density observed on expression of Rac1-Y64D might result from excessive activation of the branch-promoting WRC/Arp2/3 complex pathway. To test this hypothesis, we used RNAi to knock down expression of the WRC component Cyfip (homolog of human CYFIP1/2) in Rac1-Y64D expressing neurons. We found that Cyfip knock down rescued the morphological defects induced by Rac1-Y64D, in particular the increase in branches close to the cell body (Fig. 5A-F). We quantified dendritic architecture using Sholl analysis, and this indicated that the branching of neurons expressing Rac1-Y64D is significantly different to that of both control and Rac1-Y64D + Cyfip RNAi expressing neurons. Control neurons are not significantly different to Rac1-Y64D + Cyfip RNAi neurons, demonstrating that knockdown of Cyfip rescues the Rac1-Y64D phenotype (Fig. 5G). These results suggest that Rac1-Y64D induces defects in dendrite morphology by over-activating the WRC and that reducing WRC activity can suppress morphological defects induced by Rac1-Y64D.

Discussion

We had previously reported a number of germline *RAC1* variants as causes for RAC1-NDD.[4] The RAC1-NDD patients could be divided into broad categories according to their head circumferences. Although we presented multiple patients with either micro- or macrocephaly, we had identified only one patient, with a *RAC1* Y64D variant, located in the switch II region, with a head circumference within the normal range. We now describe a total of eight patients with missense variants resulting in five distinct substitutions of three residues within the Q61-R68 region within switch II of RAC1 (Fig. 1). These patients are characterised by variable combinations of developmental delay, intellectual disability, brain morphological defects such as polymicrogyria and cardiovascular defects (Table 1). Their phenotypic similarity with each other and absence of extreme micro- or macrocephaly distinguishes them from patients with variants in other regions of *RAC1.* Five out of eight patients described here are less than six years-of-age and patient #7 (in Table 1) was born prematurely in the 26th week of gestation. This makes

it difficult to compare the phenotypes of patients in this cohort. However, even within this group of patients with activating variants, there appears to be a substantial phenotype variability. For example, the developmental delay ranged from mild to severe and the head circumferences were between -2.2 to +3.0 SD. There were differences in severity of the clinical features of patients with identical Y64D variants, which suggests possible roles for genetic background or environmental factors in determining the phenotype of this condition.

In our original study our only functional data regarding Y64D was that it induced morphological changes in cultured fibroblasts reminiscent of those induced by constitutively active RAC1, leading us to propose that this could be an activating variant.[4] The current study considerably extends the functional understanding of this variant and others affecting nearby residues. We confirm that all of the switch II variants analysed here are activating by showing that they all increase levels of GTP-bound RAC1, all promote fibroblast spreading and all stimulate downstream signalling pathways. In our previous report we described three variants affecting residues closely flanking the region of RAC1 explored in this study (V51M, V51L and P73L) and none of these variants showed any evidence of increased RAC1 activation.[4] Overall, these observations suggest that variants affecting residues Q61-R68, form a distinct class of activating *RAC1* variants with shared mechanistic features. Activating *RAC1* mutations affecting residues outside of switch II have been identified in various cancers[24], so it is possible that the syndrome described here could potentially also be caused by variants outside of the Q61-R68 region.

Recently, a *de novo* germline E62K variant of *RAC2*, a *RAC1* paralog expressed primarily in the hematopoietic cell lineages, was shown to cause severe T- and B-cell lymphopenia, myeloid dysfunction, and recurrent respiratory infections through gain-of-function effects (OMIM 618986).[25] Interestingly, *de novo* germline Q61L and E62K variants in *RAC3* have also been shown to cause a neurodevelopmental disorder with structural brain anomalies and dysmorphic faces (OMIM 618577).[26] However, no

functional studies have yet been performed for the *RAC3* variants. Germline Y64C, R66G and R68Q variants in *CDC42*, another Rho GTPase closely related to RAC1, have been described to cause Takenouchi-Kosaki syndrome (OMIM 616737), another neurodevelopmental disorder.[27-29] Interestingly, Q61-R68 has also been identified as a somatic mutational hotspot in KRAS in colon and rectal cancers.[30] Overall, our and previous results suggest that the Q61-R68 region of switch II may be prone to activating mutations throughout the RAS superfamily.

There are two likely explanations for pathogenic switch II variants causing activation: firstly, since switch II contains residues with a direct role in GTP hydrolysis, variants that change these residues or alter their position by inducing local conformational changes are likely to reduce the efficiency of GTP hydrolysis, thus increasing the proportion of cellular RAC1 in an activated, GTP-bound state. Of the variants described here, Q61E is most likely to directly affect GTP hydrolysis since Q61 has a well-established role in the hydrolysis process.[11] Although we did not perform functional studies for the Q61E variant, this substitution has previously been shown to increase RAC1 activity.[13] The second possible mechanism is via altering interactions with regulators; for example, reduced affinity for GTPase activating proteins (GAPs) or guanine nucleotide dissociation inhibitors would be expected to increase basal activity of RAC1. For example, a E62K variant in RAC2 abolishes the ability of GAPs to accelerate GTP hydrolysis.[25] The crystal structure of RAC1 bound to the GAP *sptP* identifies Y64 as a direct point of contact between the two proteins; therefore, it is possible that Y64D and Y64C variants increase RAC1 activity by impairing interaction with GAPs.[31] R68 is predicted to form several hydrogen bonds that stabilise the structure of switch II, so substitution of this residue could impact GTP hydrolysis and/or regulator binding by inducing local structural changes. Both the R68G and R68S variants would be expected to disrupt hydrogen bonding within switch II, so while we did not functionally analyse R68S, it is likely to have a similar effect on RAC1 activity to R68G. While there are clear mechanistic similarities between

variants investigated here, the extent and nature of changes in GTP hydrolysis and protein interactions induced by each variant will differ, so their disease mechanisms are unlikely to be identical.

The increased activity observed for all of these variants is likely to be significant as increased or decreased RAC1 activation has also been detected in neurodevelopmental disorders caused by variants in *TRIO*[32] and *HACE1*,[33] supporting the notion that tight regulation of the level of RAC1 activity is important for proper neurodevelopment and function. The increase in RAC1-GTP levels we observe for Y64D, Y64C and R68G is smaller than for the constitutively active Q61L mutant, which is unable to hydrolyse GTP and is therefore always in an active state. This mirrors the relative effects of these mutants on fibroblast morphology and PAK activation and suggests that the variants found in patients are still able to undergo a GTPase cycle, albeit with a higher percentage of molecules in an active state at any one time relative to WT RAC1. This likely also applies to Q61E, which has previously been shown to activate RAC1, but less strongly than Q61L.[13] Although we did not functionally characterise every variant in this study, there is no obvious correlation between the extent of RAC1 activation in our functional studies and the severity of disease phenotypes for the variants studied.

In our *Drosophila* studies, we found that the Rac1-Y64D alters the morphology and growth of neuronal axons and dendrites. Specifically, we find that overall extension of axons and dendrites is reduced, while branching is increased. Rac1 activity is known to trigger branching of axons and dendrites,[15,20] leading us to propose that the elevated levels of active Rac1-Y64D results in increased frequency of branch initiation events at the expense of axon/dendrite extension. Disorganisation of axon fascicles in the CNS of *Drosophila* embryos expressing Rac1-Y64D is also consistent with altered axon morphology and/or pathfinding being a contributing factor in phenotypes caused by this variant. Notably, the dendritic branching phenotype induced by Rac1-Y64D can be suppressed by reducing levels of Cyfip, a specific downstream effector of Rac1 in *Drosophila* and humans and component of the WRC. This result suggests

that the Rac1-Y64D branching phenotype is caused by overactivation of the WRC/Arp2/3 complex pathway. Germline variants in the genes encoding WRC components (e.g. *CYFIP2* and *WASF1*) or for ubiquitous actins (e.g. *ACTB* and *ACTG1*) have been implicated in a variety of neurodevelopmental disorders.[4,34-39] Of note, overactivation of the WRC/Arp2/3 complex pathway has been shown to underpin NDDs caused by variants in CYFIP2.[40] As well as increasing our mechanistic understanding of the cellular and developmental effects of switch II variants, our ability to genetically rescue phenotypes induced by Rac1-Y64D identifies the WRC/Arp2/3 pathway as a possible pharmacological target for treatment of this and possibly other disorders in which RAC1 activity is elevated. However, further research is needed to explore whether these results can be reproduced in higher organisms and establish a possible therapeutic window for such interventions.

In summary, our results establish activating substitutions within the switch II region of RAC1 as a distinct cause of neurodevelopmental delay and delineate their clinical consequences, provide an insight into the underlying disease mechanism and reveal a possible therapeutic target. Furthermore, our findings suggest a potential mechanistic and therapeutic convergence between variants in RAC1 and several other related neurodevelopmental disease-genes involved in regulation of Rho-GTPases and the WRC/Arp2/3 pathway.

Contribution statement

SB and TM conceived the study and wrote the manuscript. AB, MB, GC, NA, HS and PP performed laboratory experiments. TM, SB, MGK and AM supervised experiments. SB, ER, KA-Y, LB, BD, DF, ACEH, ACJ, MAK, IK, CR, MR, NLR, JS, KS and ZLX provided the genetic and the clinical data. All authors read and approved the manuscript.

Acknowledgements and Funding

We are thankful to all patients and families for participating in the study. We are thankful to the Deciphering Developmental Disorders (DDD) study for the invaluable collaboration. The DDD Study (Cambridge South REC approval 10/H0305/83 and the Republic of Ireland REC GEN/284/12) presents independent research commissioned by the Health Innovation Challenge Fund (grant number HICF-1009-003), a parallel funding partnership between the Wellcome Trust and the Department of Health and the Wellcome Trust Sanger Institute (grant number WT098051). The views expressed in this publication are those of the author(s) and not necessarily those of the Wellcome Trust, BBSRC or the Department of Health. The research team acknowledges the support of the National Institute for Health Research, through the Comprehensive Clinical Research Network, UK. TM acknowledges financial support from the Wellcome Trust Grant no. 201958/Z/16/Z. We thank the University of Manchester Bioimaging and Fly Facilities for technical assistance.

Competing Interests

None of the authors declare any conflicts of interest.

Supplementary material

Supplementary material is available at *Brain* online.

References

1. Jaffe AB, Hall A. Rho GTPases: biochemistry and biology. *Annu Rev Cell Dev Biol*. 2005;21:247-69. doi:10.1146/annurev.cellbio.21.020604.150721
2. Stankiewicz TR, Linseman DA. Rho family GTPases: key players in neuronal development, neuronal survival, and neurodegeneration. *Front Cell Neurosci*. 2014;8:314. doi:10.3389/fncel.2014.00314
3. Karczewski KJ, Francioli LC, Tiao G, *et al*. The mutational constraint spectrum quantified from variation in 141,456 humans. *Nature*. May 2020;581(7809):434-443. doi:10.1038/s41586-020-2308-7
4. Reijnders MRF, Ansor NM, Kousi M, *et al*. RAC1 Missense Mutations in Developmental Disorders with Diverse Phenotypes. *Am J Hum Genet*. Sep 7 2017;101(3):466-477. doi:10.1016/j.ajhg.2017.08.007
5. Deciphering Developmental Disorders S. Prevalence and architecture of de novo mutations in developmental disorders. *Nature*. Feb 23 2017;542(7642):433-438. doi:10.1038/nature21062
6. Richards S, Aziz N, Bale S, *et al*. Standards and guidelines for the interpretation of sequence variants: a joint consensus recommendation of the American College of Medical Genetics and Genomics and the Association for Molecular Pathology. *Genet Med*. May 2015;17(5):405-24. doi:10.1038/gim.2015.30
7. Baker MJ, Rubio I. Active GTPase Pulldown Protocol. *Methods Mol Biol*. 2021;2262:117-135. doi:10.1007/978-1-0716-1190-6_7
8. Qu Y, Hahn I, Lees M, *et al*. Efa6 protects axons and regulates their growth and branching by inhibiting microtubule polymerisation at the cortex. *Elife*. Nov 13 2019;8doi:10.7554/eLife.50319
9. Kakanj P, Eming SA, Partridge L, Leptin M. Long-term in vivo imaging of Drosophila larvae. *Nat Protoc*. Mar 2020;15(3):1158-1187. doi:10.1038/s41596-019-0282-z
10. Worthylake DK, Rossman KL, Sondek J. Crystal structure of Rac1 in complex with the guanine nucleotide exchange region of Tiam1. *Nature*. Dec 7 2000;408(6813):682-8. doi:10.1038/35047014
11. Toma-Fukai S, Shimizu T. Structural Insights into the Regulation Mechanism of Small GTPases by GEFs. *Molecules*. Sep 11 2019;24(18)doi:10.3390/molecules24183308
12. Der CJ, Finkel T, Cooper GM. Biological and biochemical properties of human rasH genes mutated at codon 61. *Cell*. Jan 17 1986;44(1):167-76. doi:10.1016/0092-8674(86)90495-2
13. Doye A, Mettouchi A, Bossis G, *et al*. CNF1 exploits the ubiquitin-proteasome machinery to restrict Rho GTPase activation for bacterial host cell invasion. *Cell*. Nov 15 2002;111(4):553-64. doi:10.1016/s0092-8674(02)01132-7
14. Tahirovic S, Hellal F, Neukirchen D, *et al*. Rac1 regulates neuronal polarization through the WAVE complex. *J Neurosci*. May 19 2010;30(20):6930-43. doi:10.1523/JNEUROSCI.5395-09.2010
15. Sturner T, Tatarnikova A, Mueller J, *et al*. Transient localization of the Arp2/3 complex initiates neuronal dendrite branching in vivo. *Development*. Apr 4 2019;146(7)doi:10.1242/dev.171397

16. Eden S, Rohatgi R, Podtelejnikov AV, Mann M, Kirschner MW. Mechanism of regulation of WAVE1-induced actin nucleation by Rac1 and Nck. *Nature*. Aug 15 2002;418(6899):790-3. doi:10.1038/nature00859
17. Stradal TE, Rottner K, Disanza A, Confalonieri S, Innocenti M, Scita G. Regulation of actin dynamics by WASP and WAVE family proteins. *Trends Cell Biol*. Jun 2004;14(6):303-11. doi:10.1016/j.tcb.2004.04.007
18. Spillane M, Ketschek A, Jones SL, *et al*. The actin nucleating Arp2/3 complex contributes to the formation of axonal filopodia and branches through the regulation of actin patch precursors to filopodia. *Dev Neurobiol*. Sep 2011;71(9):747-58. doi:10.1002/dneu.20907
19. Kumar R, Sanawar R, Li X, Li F. Structure, biochemistry, and biology of PAK kinases. *Gene*. Mar 20 2017;605:20-31. doi:10.1016/j.gene.2016.12.014
20. Ng J, Nardine T, Harms M, *et al*. Rac GTPases control axon growth, guidance and branching. *Nature*. Mar 28 2002;416(6879):442-7. doi:10.1038/416442a
21. Luo L, Liao YJ, Jan LY, Jan YN. Distinct morphogenetic functions of similar small GTPases: Drosophila Drac1 is involved in axonal outgrowth and myoblast fusion. *Genes Dev*. Aug 1 1994;8(15):1787-802. doi:10.1101/gad.8.15.1787
22. Sanchez-Soriano N, Tear G, Whitington P, Prokop A. Drosophila as a genetic and cellular model for studies on axonal growth. *Neural Dev*. May 2 2007;2:9. doi:10.1186/1749-8104-2-9
23. Singhania A, Grueber WB. Development of the embryonic and larval peripheral nervous system of Drosophila. *Wiley Interdiscip Rev Dev Biol*. May-Jun 2014;3(3):193-210. doi:10.1002/wdev.135
24. Chang MT, Asthana S, Gao SP, *et al*. Identifying recurrent mutations in cancer reveals widespread lineage diversity and mutational specificity. *Nat Biotechnol*. Feb 2016;34(2):155-63. doi:10.1038/nbt.3391
25. Hsu AP, Donko A, Arrington ME, *et al*. Dominant activating RAC2 mutation with lymphopenia, immunodeficiency, and cytoskeletal defects. *Blood*. May 2 2019;133(18):1977-1988. doi:10.1182/blood-2018-11-886028
26. Costain G, Callewaert B, Gabriel H, *et al*. De novo missense variants in RAC3 cause a novel neurodevelopmental syndrome. *Genet Med*. Apr 2019;21(4):1021-1026. doi:10.1038/s41436-018-0323-y
27. Martinelli S, Krumbach OHF, Pantaleoni F, *et al*. Functional Dysregulation of CDC42 Causes Diverse Developmental Phenotypes. *Am J Hum Genet*. Feb 1 2018;102(2):309-320. doi:10.1016/j.ajhg.2017.12.015
28. Takenouchi T, Kosaki R, Niizuma T, Hata K, Kosaki K. Macrothrombocytopenia and developmental delay with a de novo CDC42 mutation: Yet another locus for thrombocytopenia and developmental delay. *Am J Med Genet A*. Nov 2015;167A(11):2822-5. doi:10.1002/ajmg.a.37275
29. Takenouchi T, Okamoto N, Ida S, Uehara T, Kosaki K. Further evidence of a mutation in CDC42 as a cause of a recognizable syndromic form of thrombocytopenia. *Am J Med Genet A*. Apr 2016;170A(4):852-5. doi:10.1002/ajmg.a.37526
30. Serebriiskii IG, Connelly C, Frampton G, *et al*. Comprehensive characterization of RAS mutations in colon and rectal cancers in old and young patients. *Nat Commun*. Aug 19 2019;10(1):3722. doi:10.1038/s41467-019-11530-0

31. Stebbins CE, Galan JE. Modulation of host signaling by a bacterial mimic: structure of the Salmonella effector SptP bound to Rac1. *Mol Cell*. Dec 2000;6(6):1449-60. doi:10.1016/s1097-2765(00)00141-6
32. Barbosa S, Greville-Heygate S, Bonnet M*, et al*. Opposite Modulation of RAC1 by Mutations in TRIO Is Associated with Distinct, Domain-Specific Neurodevelopmental Disorders. *Am J Hum Genet*. Mar 5 2020;106(3):338-355. doi:10.1016/j.ajhg.2020.01.018
33. Nagy V, Hollstein R, Pai TP*, et al*. HACE1 deficiency leads to structural and functional neurodevelopmental defects. *Neurol Genet*. Jun 2019;5(3):e330. doi:10.1212/NXG.0000000000000330
34. Ito Y, Carss KJ, Duarte ST*, et al*. De Novo Truncating Mutations in WASF1 Cause Intellectual Disability with Seizures. *Am J Hum Genet*. Jul 5 2018;103(1):144-153. doi:10.1016/j.ajhg.2018.06.001
35. Nakashima M, Kato M, Aoto K*, et al*. De novo hotspot variants in CYFIP2 cause early-onset epileptic encephalopathy. *Ann Neurol*. Apr 2018;83(4):794-806. doi:10.1002/ana.25208
36. Begemann A, Sticht H, Begtrup A*, et al*. New insights into the clinical and molecular spectrum of the novel CYFIP2-related neurodevelopmental disorder and impairment of the WRC-mediated actin dynamics. *Genet Med*. Nov 5 2020;doi:10.1038/s41436-020-01011-x
37. Zweier M, Begemann A, McWalter K*, et al*. Spatially clustering de novo variants in CYFIP2, encoding the cytoplasmic FMRP interacting protein 2, cause intellectual disability and seizures. *Eur J Hum Genet*. May 2019;27(5):747-759. doi:10.1038/s41431-018-0331-z
38. Riviere JB, van Bon BW, Hoischen A*, et al*. De novo mutations in the actin genes ACTB and ACTG1 cause Baraitser-Winter syndrome. *Nat Genet*. Feb 26 2012;44(4):440-4, S1-2. doi:10.1038/ng.1091
39. Cuvertino S, Stuart HM, Chandler KE*, et al*. ACTB Loss-of-Function Mutations Result in a Pleiotropic Developmental Disorder. *Am J Hum Genet*. Dec 7 2017;101(6):1021-1033. doi:10.1016/j.ajhg.2017.11.006
40. Schaks M, Reinke M, Witke W, Rottner K. Molecular Dissection of Neurodevelopmental Disorder-Causing Mutations in CYFIP2. *Cells*. May 29 2020;9(6)doi:10.3390/cells9061355
41. Hirshberg M, Stockley RW, Dodson G, Webb MR. The crystal structure of human rac1, a member of the rho-family complexed with a GTP analogue. *Nat Struct Biol*. Feb 1997;4(2):147-52. doi:10.1038/nsb0297-147

Figure legends

Figure 1. RAC1 switch II variants cause neurodevelopmental disorder. Panel A: Alignment of switch II region of RAC1 and related small GTPases. Residues in RAC1 affected by described variants indicated in red. **Panel B.** Structure of RAC1 bound to GTP analogue. Switch II coloured grey. Hydrogen bonds predicted to be formed between R68 and other residues in RAC1 shown in cyan. Structure from Hirshberg *et al*.[41] Image preparation and hydrogen bond prediction performed using UCSF ChimeraX. **Panel C.** T1-weighted brain MRI images of patient 3 with the Y64C variant illustrating bilateral perisylvian polymicrogyria (white quadrilaterals) and thin corpus callosum (arrow).

Figure 2. RAC1 switch II variants increase levels of GTP-bound RAC1 and alter fibroblast morphology. Panel A. Western blot of myc-RAC1-GTP (top panel) pulled down from lysates of HEK293 cells expressing indicated RAC1 variant using PAK-CRIB probed with anti-myc. Lower two panels show blots of raw lysates used in pulldowns probed with anti-myc to show total myc-RAC1 levels or anti-actin as loading control. Uncropped images of these blots are shown in Fig. S1. **Panel B.** Quantitation of relative GTP-RAC1 levels for indicated RAC1 variants. Calculated by dividing GTP-RAC1 band intensity by total RAC1 intensity for each sample then normalising to value obtained for constitutively active (Q61L) RAC1 in the same dataset. N = 7 independent experiments for all variants except Y64C and R68G where n=4. Data analysed in Graphpad Prism using mixed effects model. * indicated $P<0.05$. **Panel C.** Spreading NIH3T3 fibroblasts expressing indicated RAC1 variant stained with Alexa568-Phalloidin to label F-actin and anti-myc to label expressed RAC1 variant. Second row shows magnification of a section of the cell periphery in the above image. Arrows indicate localisation of RAC1 variants to cell periphery. Scale bars in first column indicate 10 µm and apply to all images in the row. **Panel D.** Circularity of cells expressing indicated RAC1 variant. N > 50 cells pooled from 3 independent experiments. Line indicates mean value. Data statistically analysed using Krustal-Wallis test with Dunn's correction for multiple comparisons.

**** p < 0.0001, *** p < 0.001, * p < 0.05, ns p > 0.05 relative to RAC1 WT. **Panel E.** Categorisation of cell morphology based on predominant protrusion type. Cell scored as >50% lamellipodia or filopodia if this protrusion type occupies greater than 50% of cell periphery. N > 50 cells pooled from 3 independent experiments. DN = dominant negative; CA = constitutively active.

Figure 3. RAC1 switch II variants increase WRC and PAK activity. Panel A,B. Spreading NIH3T3 fibroblasts expressing indicated RAC1 variant stained for WAVE2 (Panel A) or activated PAK1/2/3 (Panel B). Top row in each panel shows staining for WAVE2 or activated PAK1/2/3 alone. Middle row shows a merge or WAVE2 or activated PAK1/2/3 (magenta) and myc-RAC1 (green) channels and bottom row shows a magnification of a region of cell periphery from above merged images. Arrows indicate peripheral accumulations of WAVE2 or activated PAK1/2/3. Scale bars in first column indicate 10 µm and apply to all images in the row. **Panel E.** Sctivated PAK fluorescence intensity at cell periphery of NIH3T3 cells expressing indicated variant. N > 50 cells pooled from 3 independent experiments. Line indicates mean value. Data statistically analysed using Krustal-Wallis test with Dunn's correction for multiple comparisons. **** p < 0.0001, ns p > 0.05 relative to RAC1 WT. DN = dominant negative; CA = constitutively active.

Figure 4. Expression of Rac1-Y64D alters axon morphology and organization in *Drosophila* embryos. Panel A: Representative images of cultured *Drosophila* embryonic neurons extracted from stage 11 embryos of indicated genotype. Stained for tubulin (red), F-actin (green) and DAPI (blue). Arrows indicate filopodia. Scale bar indicates 10 µm and applies to all three images. **Panel B,C:** Quantitation of axon length of cultured *Drosophila* embryonic neurons and density of filopodia along axon shaft. 85 neurons analysed for each genotype extracted from 24 stage 11 embryos. Lines indicate mean values. Data statistically analysed using Krustal-Wallis test with Dunn's correction for multiple comparisons. * p < 0.05, **** p < 0.0001, ns p > 0.05 relative to control. **Panel D:** Representative images of ventral nerve

cord of stage 16 embryos with indicated genotype stained with anti-FasII to reveal axon fasciculation in developing CNS. Lower panels show magnified region from upper panels. Arrowheads show defasciculation and asterisks show fascicule breaks. Scale bars in first column indicate 10 µm and apply to all images in the row. **Panel E:** Quantitation of number of segments in which fasciculation defects are observed ventral nerve cord of in stage 16 FasII stained embryos. At least 19 embryos analysed for each genotype. Lines indicate mean values. Data statistically analysed using Krustal-Wallis with Dunn's correction for multiple comparisons. **** $p < 0.0001$, ns $p > 0.05$ relative to control.

Figure 5. Expression of Rac1-Y64D alters dendritic branching in *Drosophila* sensory neurons. Panels A-C. Class IVda sensory neurons from dorsal surface of segments A1-A4 of L3 larvae of indicated genotype. Neurons visualized using CD8-mCherry expressing under the control of ppk-Gal4. Scale bar indicates 40 µm and applies to all three images. **Panels D-F.** Magnification of the area around the cell body for the cells shown in panels A-C. Scale bar indicates 40 µm and applies to all three images. **Panel G.** Sholl analysis of dendritic organization in which the number of times dendrites intercept a semicircle originating at the cell body is plotted against the radius of the semicircle. The semicircle comprises the region of the neuron that is dorsal to the cell body, corresponding to approximately the top half of the images shown in panels A-C. Graph shows mean +/- SEM of ~ 15 neurons for each data set. Statistical analysis by two-way ANOVA. **** $p < 0.0001$, ns $p > 0.05$ relative to control.

1 **Table 1 Clinical features of patients with activating *RAC1* variants in switch II region**

Patient #	**1 (This study)**	**2 (Reijnders et al 2017 AJHG)**	**3 (This study)**	**4 (This study)**	**5 (This study)**	**6 (This study)**	**7 (This study)**	**8 (This study)**
Sex, age t	Female, 2y6m	Male, 12y	Female, 5y	Male, 14y	Female, 3y9m	Female, 3y	Female, 5y	Male, 15y
RAC1 variant[a]	*De novo* c.181C>G (p.(Gln61Glu))	*De novo* c.190T>G (p.(Tyr64Asp))	c.190T>G (p.(Tyr64Asp))[b]	*De novo* c.190T>G (p.(Tyr64Asp))	*De novo* c.190T>G (p.(Tyr64Asp))	*De novo* c.191A>G (p.(Tyr64Cys))	c.202C>A (p.(Arg68Ser))[b]	c.202C>G (p.(Arg68Gly))[c]
Significant prenatal, birth or neonatal history	Neonatal feeding difficulties	One of non-identical twins. Mild neonatal hypotonia.	None	None	None	RSV bronchiolitis at age 1m	Born at 25w 4d. Neonatal feeding difficulties. Grade I IVH	Neonatal hypotonia
Height (age) (SD)	95.9cm (2y6m) (+1.6)	159.4cm (12y) (+0.9)	88.6cm (3y4m) (−2.2)	165cm (14y) (+0.3)	93.5cm (3y9m) (−1.4)	87.5cm (3y) (−1.7)	95.5cm (5y1m) (+2.9)	148.5cm (13y) (−0.8)
Weight (age) (SD)	24.4 kg (2y6m) (+5.0)	Unknown	11.7kg (3y4m) (−2.0)	65kg (14y) (+1.4)	11.7kg (3y9m) (−2.5)	10.1kg (3y) (−3.2)	14.2kg (5y2m) (−2.2)	33.4kg (13y) (−1.5)
OFC cm (age) (SD)	47.4cm (2y6m) (−2.0)	56.5cm (12y) (+0.7)	50.8cm (5y) (−0.8)	61.5cm (14y) (+3.1)	49cm (3y9m) (+0.2)	49.0cm (22m) (−1.6)	45.7cm (4y5m) (−2.2)	54cm (13y) (−0.9)
Independent sitting	10m	19m	Unknown	Unknown	Delayed	Unknown	12m	Unknown
Independent walking	20m	4y	Unknown	2y6m	1y6m	1y6m	2y	3y
DD or ID	Mild-moderate	Severe	Moderate	Mild	Mild	Mild	Mild	Moderate
Behavioural and neurological features	Eating disorder	Hand stereotypies	Hypotonia and poor balance	Autistic features, dyspraxia, ADHD	Sleep difficulties	None	Hypotonia, poor motor coordination, frequent falls, stereotypies	Mild sensory issues and hypotonia
Brain MRI features	Normal	PMG	Not performed	Chiari I malformation	Not performed	Bilateral PMG, thin CC, thin WM	Short CC, prominent superior vermis fissures and 4th ventricular outlet	Bilateral CP cysts, prominent perivascular spaces, increased WM T2 flair signal intensity
Vision or	Normal	Mild visual	Normal	Unilateral	Chronic	Unilateral	Anisocoria,	Recurrent

hearing features		impairment, bilateral SNHL		mild-moderate SNHL	OM, mild-moderate CHL	congenital cataract	ROP	middle ear effusions
CVS features	ASD, VSD	VSD	None	Unknown	VSD	None	PDA, PFO, TI	None
Craniofacial features	Normal	Prominent metopic suture and nasal bridge, wave shaped PFs, low columella, dysplastic ears, high palate	Prominent glabella, macrostomia, micrognathia	Hypertelorism, high palate	Prominent arched eyebrows, dysplastic helices, bulbous nasal tip, short columella	Prominent glabella, mild hypertelorism, epicanthus	Prominent forehead, arched eyebrows, macrostomia	Arched eyebrows, broad nasal bridge, broad uvula, retrognathia
Other observations	Keratosis pilaris, miliaria	Long-thin fingers, fetal finger pads, pes planus	None	Nocturnal enuresis, KFS, mild S-shaped scoliosis, mild joint laxity	Recurrent papular urticaria, bilateral 5th digit clinodactyly	Long fingers, fetal finger pads, short neck, pectus excavatum, thoracal kyphosis	Bilateral nodules on heels, gastrostomy feeding, GOR, constipation, CLD	Dysfunctional voiding, thenar hypoplasia, dental caries, constipation

Key: ADHD attention deficit hyperactivity disorder; CC corpus callosum, CHL conductive hearing loss; CLD chronic lung disease; CP choroid plexus; CVS cardiovascular; d days; DD developmental delay; GOR gastro-oesophageal reflux; ID intellectual disability; IVH intraventricular haemorrhage; KFS Klippel-Feil syndrome, m months; OFC occipitofrontal circumference; OM otitis media; PDA Patent ductus areterios, PFs palpebral fissures, PFO patent foramen ovale; PMG polymicrogyria; ROP retinopathy of prematurity; RSV respiratory syncytial virus; SNHL sensorineural hearing loss; TI tricuspid valve insufficiency; w weeks; WM white matter.

[a]NM_006908.4.

[b]Both parents not available for testing.

[c]Variant not present in mother and father not available for testing.

Table 2 Group-wise comparison of selected clinical features of RAC1-NDD patients

Group	Q61-R68 RAC1-NDD	V51 RAC1-NDD	All other RAC1-NDD
Variants	Q61E, Y64C, Y64D, R68S, R68G	V51L, V52M	C18Y, N39S, P73L, C157Y
Number of individuals	8	2	4
Head circumference SD	−2.2 to +3.06	+4.1 to +4.5	−2.5 to −5.0
Epilepsy	None	None	2
Main brain MRI findings	Polymicrogyria in 2; Chiari I malformation in 1; thin white matter and corpus callosum in 1	White matter anomalies in 2	Cerebellar anomalies, thin corpus callosum and mega cisterna magna in 3; enlarged lateral or 4th ventricles in 2; thin brain stem in 2;

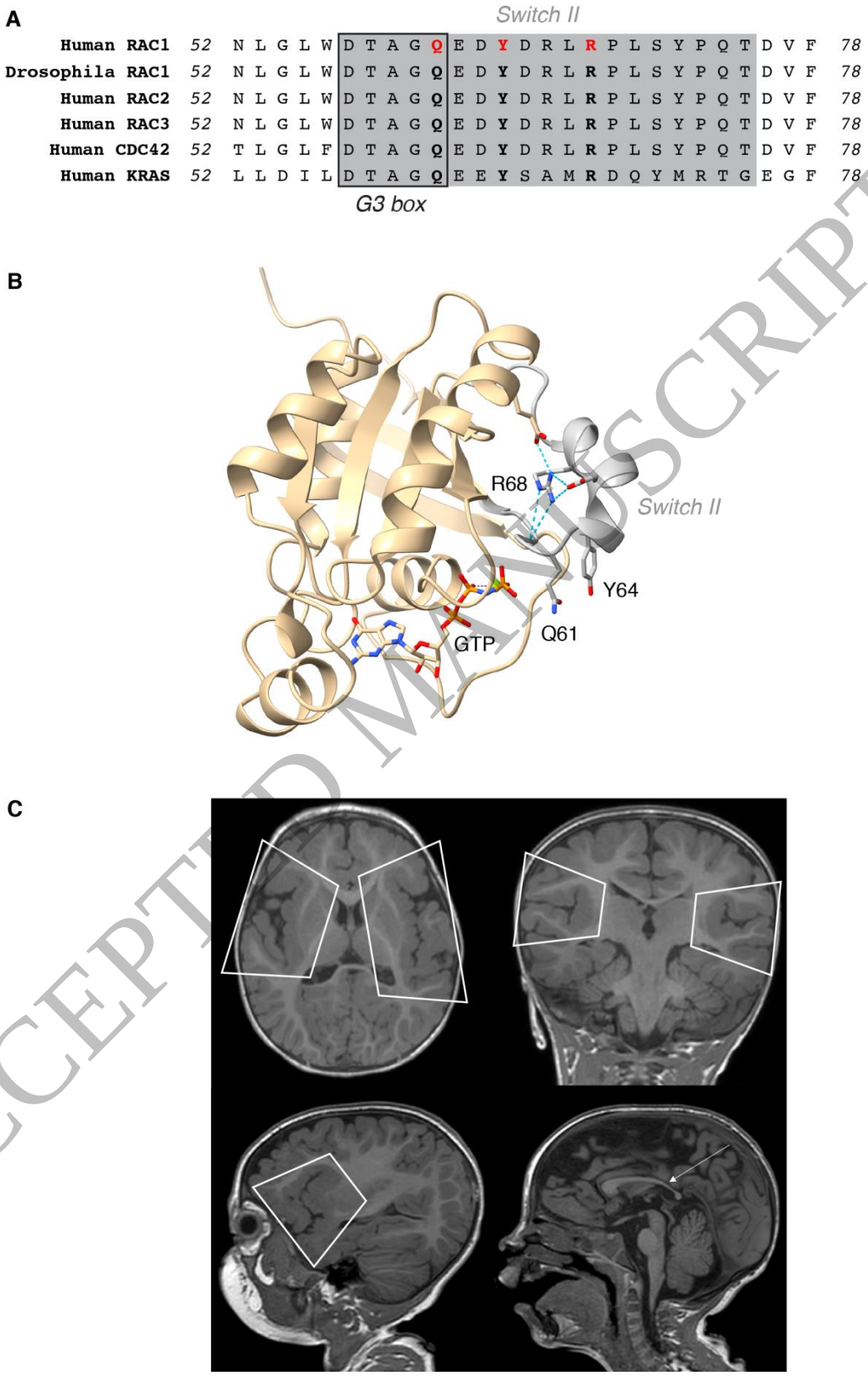

Figure 1
173x263 mm (6.2 x DPI)

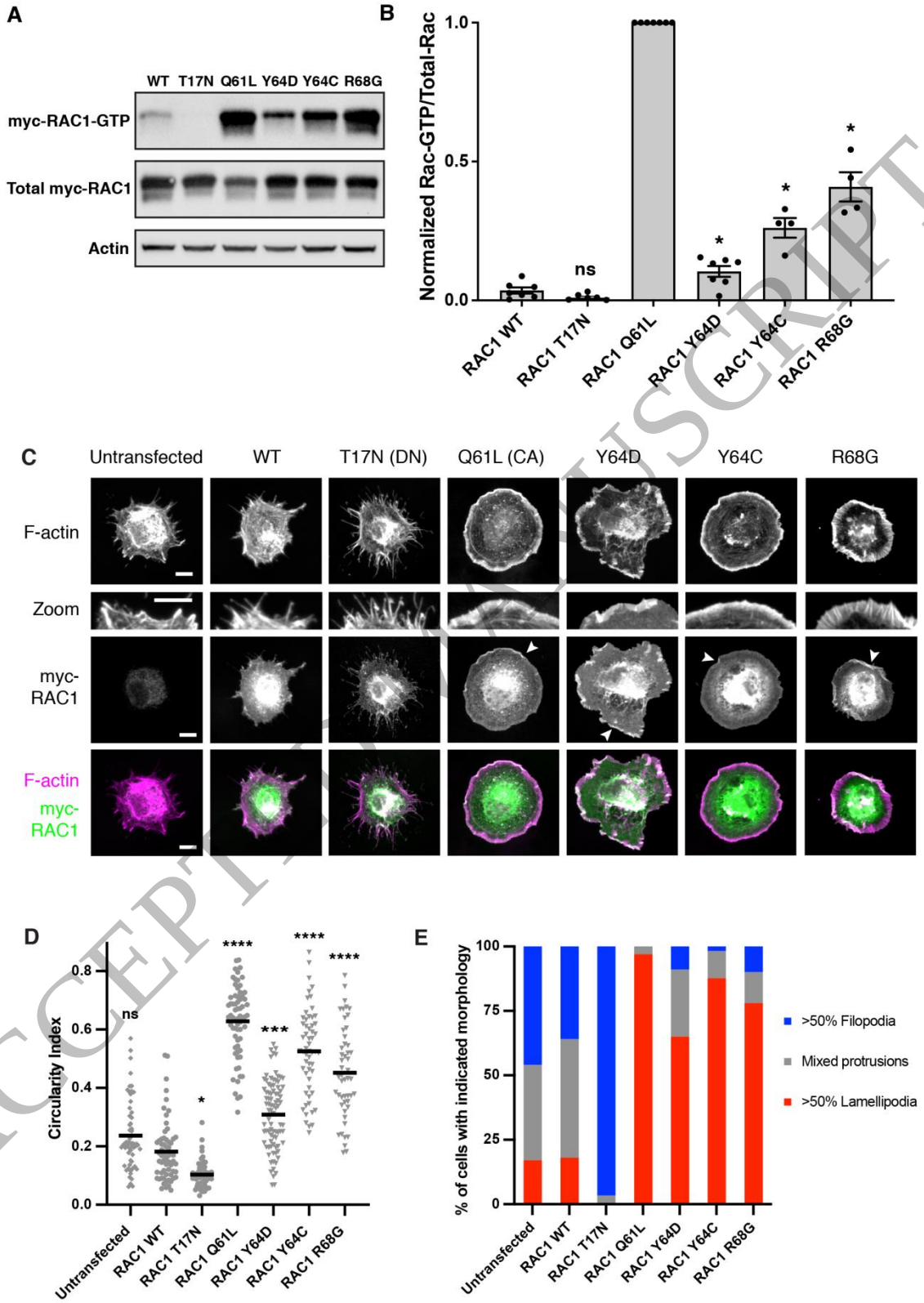

Figure 2
187x258 mm (6.2 x DPI)

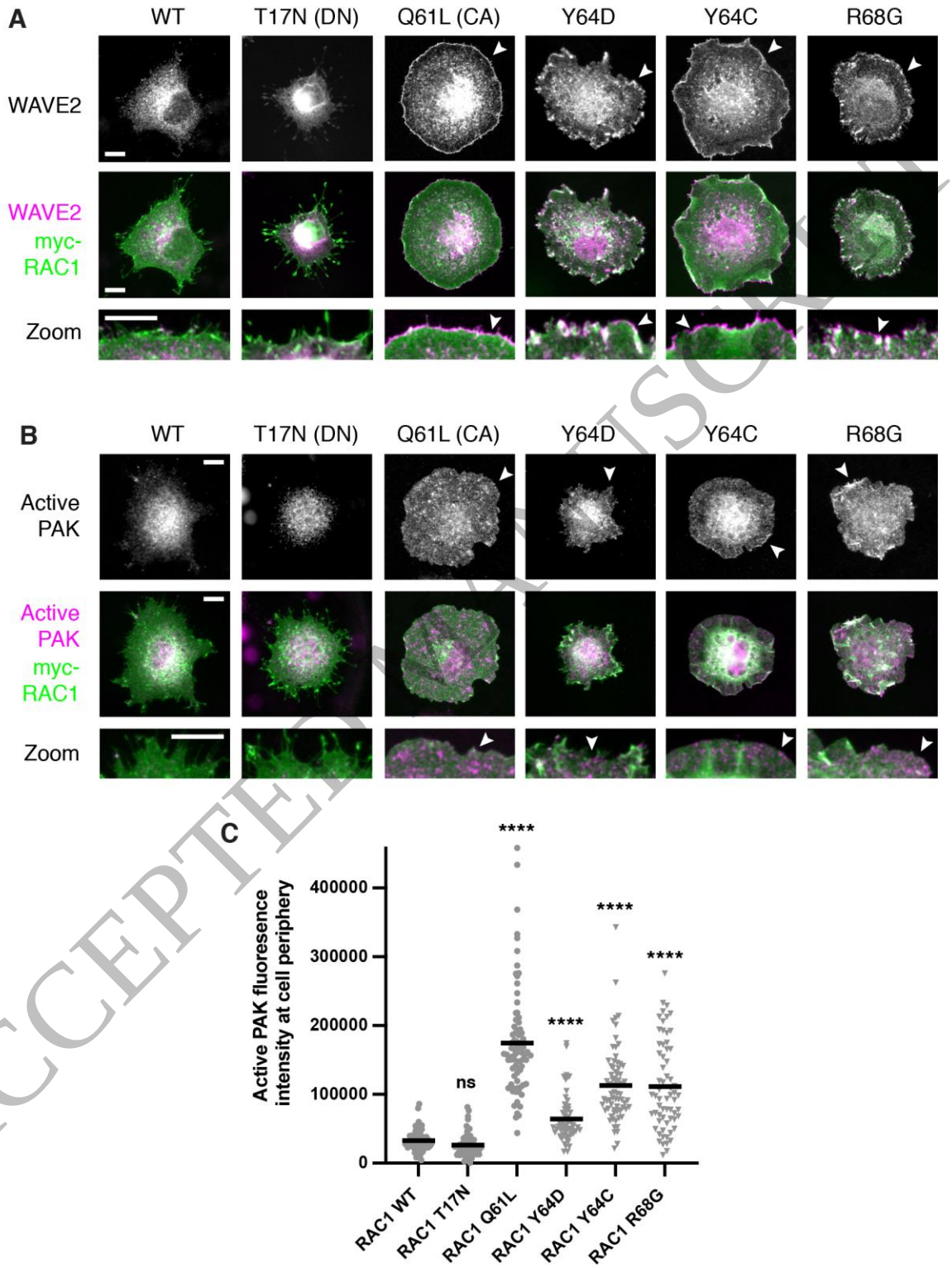

Figure 3
157x212 mm (6.2 x DPI)

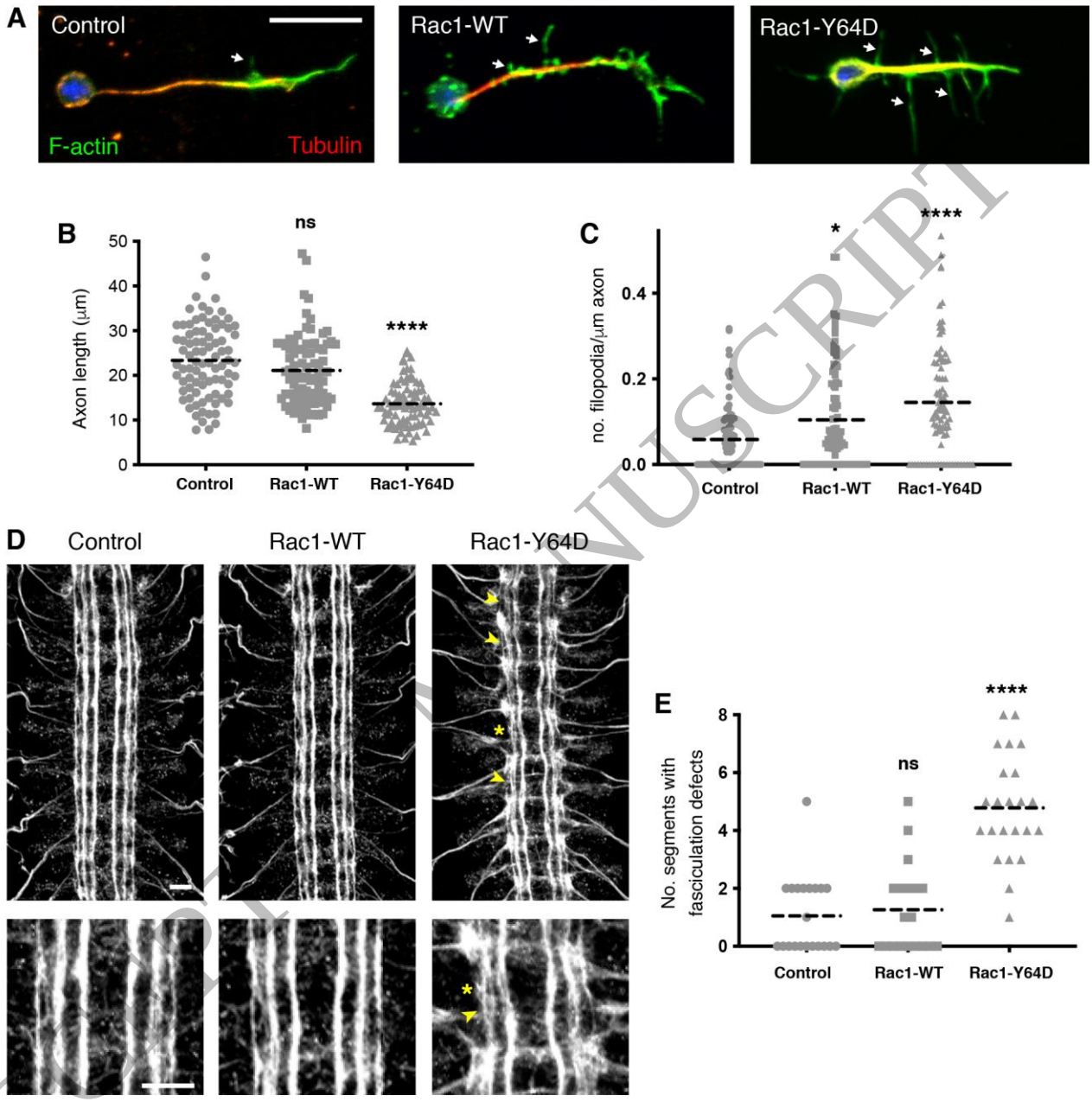

Figure 4
174x173 mm (6.2 x DPI)

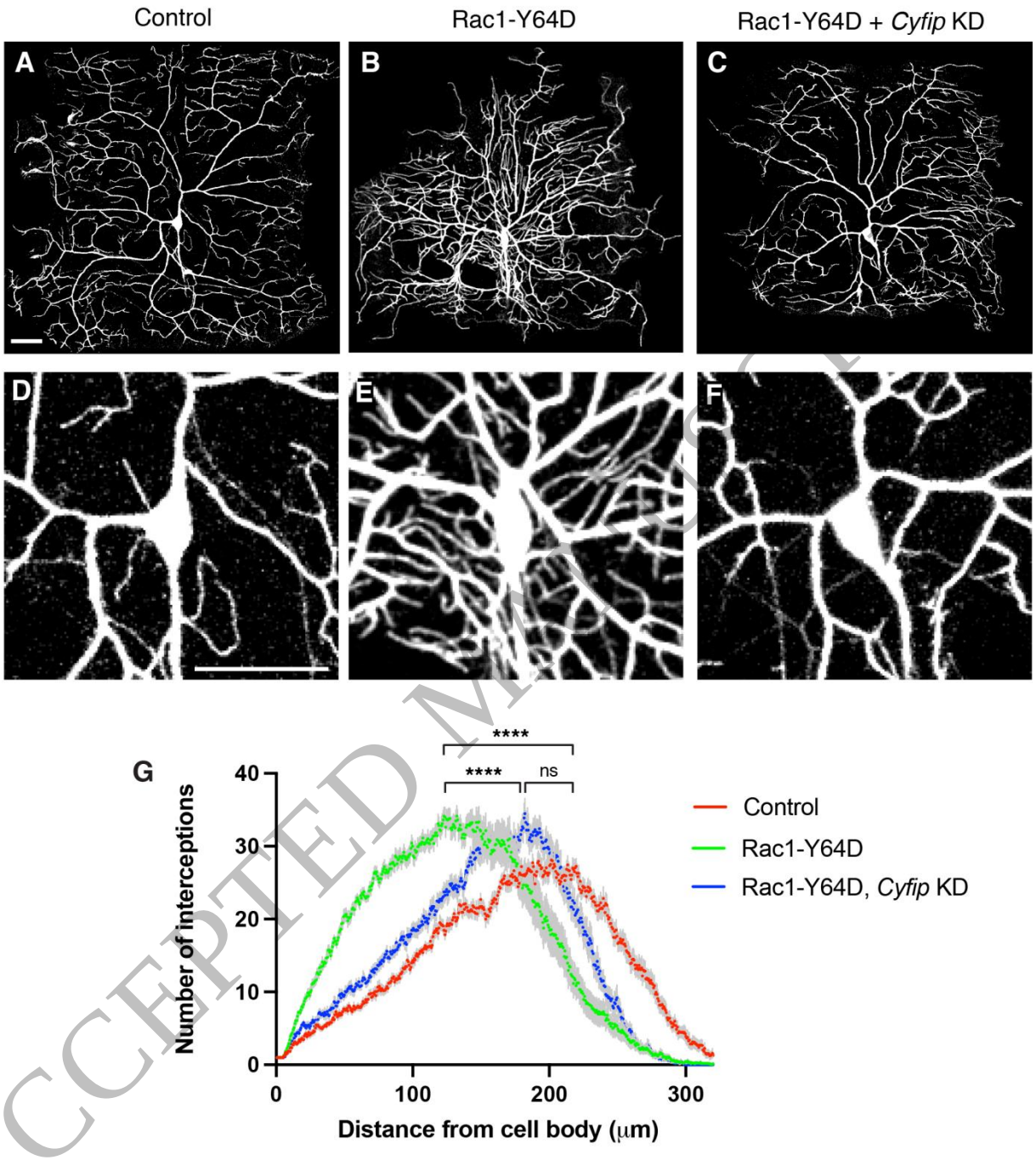

Figure 5
186x205 mm (6.2 x DPI)